Observations of Mercury's northern cusp region with MESSENGER's Magnetometer

Reka M. Winslow,[1] Catherine L. Johnson,[1,2] Brian J. Anderson,[3] Haje Korth,[3] James A. Slavin,[4] Michael E. Purucker,[5] and Sean C. Solomon[6]

Received 23 February 2012; revised 28 March 2012; accepted 29 March 2012; published 28 April 2012.

[1] The magnetic cusp of a planetary magnetosphere allows solar wind plasma to gain access to the planet's magnetosphere and, for Mercury, the surface. From measurements by the MESSENGER Magnetometer we have characterized the magnetic field in the northern cusp region of Mercury. The first six months of orbital measurements indicate a mean latitudinal extent of the cusp of ∼11°, and a mean local time extent of 4.5 hrs, at spacecraft altitudes. From the average magnetic pressure deficit in the cusp, we estimate that $(1.1 \pm 0.6) \times 10^{24}$ protons s^{-1} bombard the surface over an area of $(5.2 \pm 1.6) \times 10^{11}$ m^2 near the northern cusp. Plasma pressures in the cusp are 40% higher when the interplanetary magnetic field (IMF) is anti-sunward than when it is sunward. The influence of the IMF direction does not overcome the north-south asymmetry of Mercury's internal field, and particle flux to the surface near the southern cusp is predicted to be a factor of 4 greater than in the north. The higher particle flux impacting the surface in the south should lead to a greater exospheric source from the south and a higher rate of space weathering than in the area of the northern cusp.
Citation: Winslow, R. M., C. L. Johnson, B. J. Anderson, H. Korth, J. A. Slavin, M. E. Purucker, and S. C. Solomon (2012), Observations of Mercury's northern cusp region with MESSENGER's Magnetometer, *Geophys. Res. Lett.*, *39*, L08112, doi:10.1029/2012GL051472.

1. Introduction

[2] The magnetospheres of planets with dipolar internal fields possess magnetic cusps, regions near the magnetic poles at which fields from magnetopause currents nearly cancel the internal field. For vacuum superposition of the magnetic fields of the dipole and magnetopause currents, the cusps are topological singularities where the magnetic field vanishes. The weak field near the cusp allows the shocked solar wind plasma of the magnetosheath ready access to the magnetosphere, and the magnetic field lines that thread the cusp are populated with this plasma.

[3] Mercury's internal field is symmetric about the rotation axis but asymmetric about the geographic equator and can be represented by a dipole with a moment of 195 nT R_M^3 (where R_M is Mercury's mean radius, 2440 km) offset 0.2 R_M northward from the planetary center [*Anderson et al.*, 2011]. The high-latitude field at the surface is predicted to be 4 times weaker in the southern hemisphere than in the northern hemisphere, leading to a correspondingly greater spatial extent of the cusp projection to the surface in the south than in the north. Solar wind sputtering of species from the planetary surface may be a substantial source of exospheric particles [e.g., *Massetti et al.*, 2003]. It is not known whether asymmetric particle bombardment of the surface and corresponding differences in space weathering rates could have produced detectable hemispheric differences in surface color or reflectance.

[4] Earth's cusps have been extensively studied at low and high altitudes [e.g., *Smith and Lockwood*, 1996]. The position and size of the cusp areas at Earth depend on the solar wind pressure [*Newell and Meng*, 1994; *Zhou et al.*, 2000] and the interplanetary magnetic field (IMF) [e.g., *Newell et al.*, 1989; *Zhou and Russell*, 1997; *Lavraud et al.*, 2005]. Mercury lacks an ionosphere, the magnetosphere is a factor of ∼8 smaller than Earth's relative to the planetary diameter, and the average solar wind density is an order of magnitude higher than at Earth [*Korth et al.*, 2011a], so the cusps at Mercury may be quite different from those at Earth. In addition, because the IMF is dominantly sunward or anti-sunward at Mercury, the IMF component in the Sun-Mercury direction may play a prominent role in the dynamics of Mercury's cusps [e.g., *Sarantos et al.*, 2001].

[5] Previous work on Mercury's cusps focused on magnetosphere–solar wind interaction by means of analytic models [*Massetti et al.*, 2007; *Sarantos et al.*, 2007; *Delcourt et al.*, 2003], global magnetohydrodynamic models [*Kabin et al.*, 2000; *Ip and Kopp*, 2002], hybrid simulations [*Kallio and Janhunen*, 2003; *Omidi et al.*, 2006; *Trávníček et al.*, 2007], or semi-empirical models [*Massetti et al.*, 2003; *Mura et al.*, 2005]. These studies indicated that solar wind ions can reach the surface in the cusp region, but the spatial extent of the cusp and the particle fluence vary among the models. This variation is partly due to the different IMF and solar wind conditions assumed. From solar wind and IMF conditions at Mercury's aphelion and perihelion, *Sarantos et al.* [2007] predicted that the largest flux of precipitating solar wind ions impacting Mercury's surface occurs at local noon between 40° and 60° latitude with an equatorward shift at perihelion. To date there have been no observations that quantify the total plasma pressure in Mercury's cusps or

[1]Department of Earth and Ocean Sciences, University of British Columbia, Vancouver, British Columbia, Canada.
[2]Planetary Science Institute, Tucson, Arizona, USA.
[3]Johns Hopkins University Applied Physics Laboratory, Laurel, Maryland, USA.
[4]Department of Atmospheric, Oceanic and Space Sciences, University of Michigan, Ann Arbor, Michigan, USA.
[5]NASA Goddard Space Flight Center, Greenbelt, Maryland, USA.
[6]Department of Terrestrial Magnetism, Carnegie Institution of Washington, Washington, D. C., USA.

Corresponding Author: R. M. Winslow, Department of Earth and Ocean Sciences, University of British Columbia, 6339 Stores Rd., Vancouver, BC V6T 1Z4, Canada. (rwinslow@eos.ubc.ca)

0094-8276/12/2012GL051472

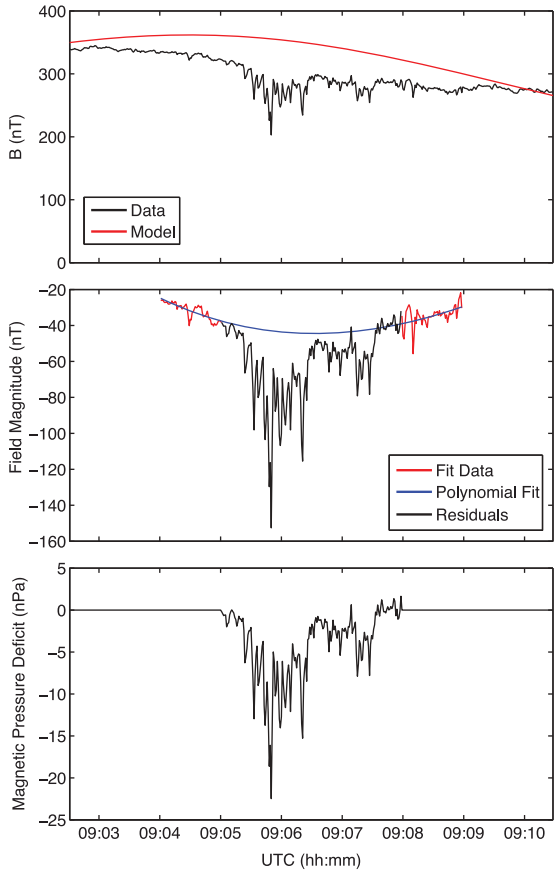

Figure 1. Example of a cusp observation on 21 August 2011, orbit 313. (top) Measured (black) and modeled (red) magnetic field magnitude in the cusp region. (middle) Magnetic depression in the residual |**B**| (black), residual data before and after cusp entry (red), and a third-degree polynomial fit (blue) to the red curve. (bottom) The calculated pressure deficit ($-P_{\mathrm{Plasma}}$).

provide a basis for assessing its sensitivity to the sunward IMF component.

[6] Orbital observations by the MErcury Surface, Space ENvironment, GEochemistry, and Ranging (MESSENGER) spacecraft's Fast Imaging Plasma Spectrometer (FIPS) have revealed that the flux of heavy ions in Mercury's magnetosphere peaks between 65° and 75° latitude, consistent with the predicted location of the northern magnetic cusp [*Zurbuchen et al.*, 2011]. The ion flux peaks coincide with depressions in magnetic field strength [*Korth et al.*, 2011b] measured with the MESSENGER Magnetometer (MAG) [*Anderson et al.*, 2007]. In this paper we characterize the northern cusp with MAG data from six months of orbital observations, calculate the corresponding surface precipitation, and investigate the influence of the sunward IMF and solar wind pressure on the mean cusp plasma pressure.

2. Observations and Data Analysis

[7] The MESSENGER spacecraft was inserted into orbit about Mercury on 18 March 2011. The initial orbit had a 200 km periapsis altitude, 82.5° inclination, 15,300 km apoapsis altitude, and 12 hour period. We use two Mercury years of MAG data starting from 23 March 2011, providing coverage at all local times. Data were analyzed in Mercury solar orbital (MSO) coordinates, for which $+X$ is sunward, $+Z$ is northward, and $+Y$ completes the right-handed system.

[8] The cusp was identified from depressions in the magnitude of 1-s averaged total-field data from which a model field had been subtracted. The model incorporates the offset internal dipole field and the magnetopause and tail fields of the *Alexeev et al.* [2010] paraboloid magnetospheric model, with model parameters given by *Anderson et al.* [2011]. An aberration correction was calculated from Mercury's orbital speed and a mean solar wind speed of 405 km s^{-1}. For each orbit exhibiting a dayside magnetic depression poleward of the magnetopause, we identified the times of the cusp outer and inner entry and exit points. Transits in the cusp were indicated by sustained depressions in the magnitude of the magnetic field **B** that exceeded typical variability and lasted several minutes. An outer cusp entry was identified at the point where the first transient decrease in |**B**| was seen, and the inner entry was picked where the sustained depression in |**B**| started. Similar criteria were used for the exit inner and outer points. Figure 1 shows the dayside depression in the total residual between the observed and model fields, given by $|\mathbf{B}|_{\mathrm{res}} = |\mathbf{B}|_{\mathrm{obs}} - |\mathbf{B}|_{\mathrm{model}}$. The orbit does not always intersect the cusp, particularly when periapsis is on the nightside, and magnetic depressions were seen on 169 of the 279 orbits analyzed. Each entry and exit time and the aberrated MSO spacecraft positions are given in Table S1 in the auxiliary material.[1] The field depressions were generally associated with enhanced magnetic fluctuations at 1–10 Hz frequency, consistent with greater intensities of local plasma instabilities. The proton gyrofrequency is 2 to 6 Hz for field strengths observed in the cusp (150 to 400 nT). The cusp entry and exit times changed by less than a few seconds for different magnetospheric model parameters.

[9] We conducted superposed epoch analyses (SEA) of |**B**| and $|\mathbf{B}|_{\mathrm{res}}$ in the cusp to derive an average magnetic depression signature (Figure 2). Individual profiles from different orbits were aligned in time on their respective cusp interval midpoints and averaged over a time span of six minutes on either side of this midpoint. We also conducted SEA of the 1–10 Hz fluctuations. The fluctuation intensity was evaluated from the 20 sample/s data by taking the root mean square (RMS) value over 1-s intervals in the direction parallel to and two components perpendicular to the 1-s averaged field direction, denoted by $\delta B_{\parallel}$, $\delta B_{\perp 1}$ and $\delta B_{\perp 2}$, respectively. We define $\delta B_{\perp} = \sqrt{(\delta B_{\perp 1}^2 + \delta B_{\perp 2}^2)}/\sqrt{2}$, so that $\delta B_{\perp} = \delta B_{\parallel}$ if the fluctuations are equal in all components. These analyses confirm the depression in the magnetic field over the cusp and show that this signature is accompanied by an increase in the magnetic fluctuations. The ratio $\delta B_{\perp}/\delta B_{\parallel}$ is about 1.5 in the cusp and higher on either side of the cusp (Figure 2), indicating that although the fluctuations in the cusp are transverse, they are less so than the adjacent lower-amplitude fluctuations.

[10] We calculated a plasma pressure that balances the magnetic field depression from $P_{\mathrm{Total}} = P_{\mathrm{Mag}} + P_{\mathrm{Plasma}}$, where P_{Total} is the total pressure; P_{Mag} is the magnetic pressure, $B^2/(2\,\mu_0)$, where μ_0 is the magnetic permeability; and P_{Plasma} is the particle thermal pressure. We estimated P_{Total} from the magnetic field removed from the cusp magnetic field

[1]Auxiliary materials are available in the HTML. doi:10.1029/2012GL051472.

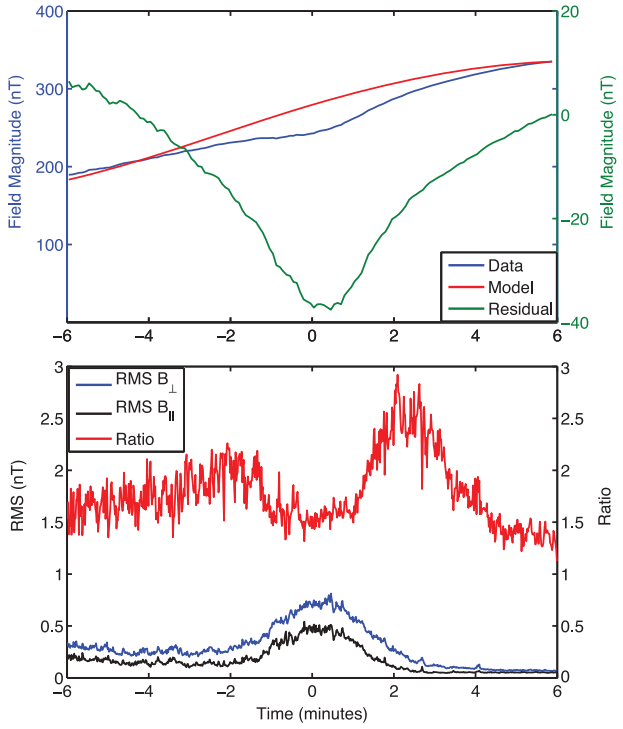

Figure 2. (top) SEA of observed |**B**| (blue) and model |**B**| (red) indicated by the scale on the left-hand ordinate, and SEA of residual |**B**| (green) indicated by the scale on the right-hand ordinate, for all 169 cusp profiles. (bottom) SEA of RMS 1–10 Hz fluctuations perpendicular and parallel to the local field, $\delta B_{\perp}$ (blue), and $\delta B_{||}$ (black) (scale on left). The red curve shows $\delta B_{\perp}/\delta B_{||}$ (scale on right).

depression [*Korth et al.*, 2011b]. The unperturbed magnetic field was determined for each pass from the magnetospheric model field and a third-degree polynomial fit to the residuals one minute before and after but excluding the depression interval (Figure 1, middle). The boundaries of the depression intervals were taken as the average of the inner and outer cusp entry or exit times. In some cases the polynomial fit did not consistently remain above the residual field magnitude in the cusp. These fits were rejected, and new fits were obtained by increasing the time interval for the baseline fit. The polynomial fit was added to the magnetospheric model field to estimate the unperturbed total magnetic field, B_U. We then evaluated $P_{Total} = B_U^2/(2\ \mu_0)$ and the magnetic pressure deficit, $P_{B\text{-deficit}} = P_{Mag} - P_{Total} = -P_{Plasma}$. This latter quantity gives the additional plasma pressure in the cusp relative to any background plasma pressure in the magnetosphere. In general, FIPS data do not show substantial proton counts adjacent to, but outside, the cusp, indicating that the background plasma pressure near the cusp is much lower than that in the cusp.

[11] The limits of the northern cusp are 55.8° and 83.6° MSO latitude and 7.2 h and 15.9 h local time. On average the cusp is approximately symmetric about noon (Figure 3). Since the MESSENGER orbit is eccentric and periapsis is on the descending latitude portion of the orbit, the cusp is encountered at lower altitudes on the descending than on the ascending orbit track. At higher altitude the cusp is on average a few degrees equatorward of that seen at lower altitude. In the magnetosphere model, the magnetic field at the magnetopause vanishes near 62°N at noon, consistent with the expected shift in cusp latitude closer to the magnetopause.

3. Discussion

[12] The observations indicate that Mercury's northern cusp region is a persistent but dynamic feature. Not only is the cusp pressure deficit variable on a given pass (Figure 1), but the cusp extent and plasma pressure can vary markedly from one orbit to the next (Figure 3). This variability likely results from the influence of different IMF and solar wind conditions and the corresponding interactions with, and dynamics of, Mercury's magnetosphere. Here we focus on establishing the mean cusp pressure and particle fluence to the surface since the plasma pressure may have important consequences for exospheric processes and space weathering. We use MESSENGER averages of IMF B_X and predictions of the solar wind ram pressure from the ENLIL solar wind model [*Odstrcil*, 2003]. Statistics of these quantities for the cusp transits are given in Table 1.

[13] MESSENGER's 12-h eccentric orbit presents challenges to analyzing the effects of the solar wind on the cusp. First, the local time extent of the cusp is sampled only twice each Mercury year (Figure 3). A study of variations in cusp local time extent with solar wind conditions will require considerably more observations than are presently available. Second, IMF conditions for a given orbit are estimated from averages of MAG observations upstream of the bow shock. The 1-h time spans for these averages are comparable to the typical time between MESSENGER cusp transits and residence in the solar wind. Only the IMF *X*-

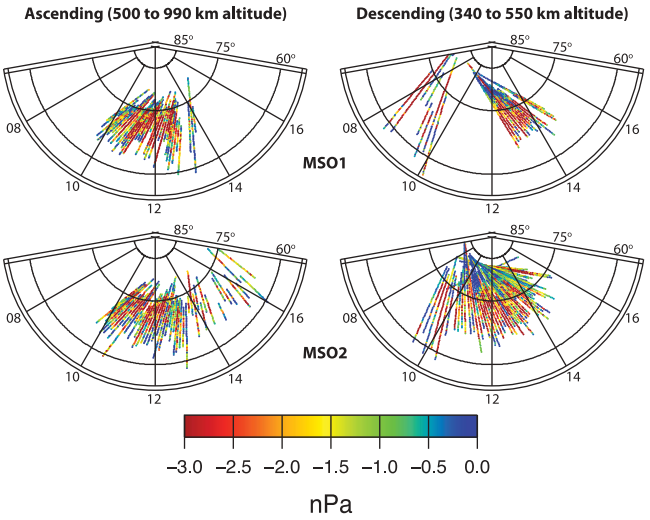

Figure 3. Stereographic projections of the pressure deficit ($-P_{Plasma}$) along each cusp profile in aberrated MSO coordinates. During portions of MESSENGER's first Mercury year in orbit (MSO1), the Magnetometer was off when the spacecraft experienced long eclipses or was close to the planet, resulting in the gap in data coverage (between ~10 h and ~12 h in local time) for the descending tracks. Complete coverage was obtained during MESSENGER's second Mercury year in orbit (MSO2). Projections span local times from 6.67 h to 17.3 h and latitudes 55°N to the pole. The color bar is saturated so that observed, but localized, pressure deficits greater in magnitude than −3 nPa are shown in red.

Table 1. Average Cusp Properties and Ambient Conditions Separated by Ascending/Descending Tracks and by the Sign of IMF B_X[a]

	IMF $B_X > 0$	IMF $B_X < 0$
	Ascending Tracks	
$\|\mathbf{B}\|$	193 nT	179 nT
P_{Plasma}	1.5 ± 0.1 nPa	2.1 ± 0.1 nPa
IMF B_X	16.4 ± 1.1 nT (σ = 5.0 nT)	−9.1 ± 0.7 nT (σ = 4.7 nT)
IMF B_Y	−4.6 ± 1.2 nT (σ = 6.0 nT)	5.9 ± 1.1 nT (σ = 5.9 nT)
IMF B_Z	1.9 ± 1.1 nT (σ = 6.3 nT)	1.3 ± 0.9 nT (σ = 6.8 nT)
P_{Ram}	11.9 ± 0.4 nPa	11.3 ± 0.4 nPa
# of orbits	45	43
Latitude	70.9° N	71.4° N
Altitude	684 km	706 km
	Descending Tracks	
$\|\mathbf{B}\|$	305 nT	318 nT
P_{Plasma}	1.8 ± 0.1 nPa	1.9 ± 0.1 nPa
IMF B_X	17.8 ± 0.9 nT (σ = 5.2 nT)	−10.7 ± 2.0 nT (σ = 5.0 nT)
IMF B_Y	−5.1 ± 1.1 nT (σ = 7.0 nT)	2.5 ± 1.4 nT (σ = 6.7 nT)
IMF B_Z	1.5 ± 0.8 nT (σ = 7.6 nT)	−0.02 ± 1.35 nT (σ = 7.0 nT)
P_{Ram}	14.5 ± 0.5 nPa	11.4 ± 0.3 nPa
# of orbits	55	26
Latitude	72.5°N	75.2°N
Altitude	426 km	404 km

[a]The mean $|\mathbf{B}|$ and P_{Plasma} inferred from decreased magnetic field strength are evaluated in the cusp. The average IMF B_X, B_Y, and B_Z are calculated from observations before and after each magnetospheric transit, and the solar wind P_{Ram} is from the ENLIL model evaluated during times of passage in the cusp. Mean cusp latitude and altitude are weighted by P_{Plasma}; the rest of the values are unweighted. Uncertainties are 1 standard error of the mean. For IMF averages, the mean standard deviation (σ) is given in parentheses; only the average B_X is consistently greater in magnitude than its variability.

component is generally larger in magnitude than its variability (Table 1), implying that the IMF averages are appropriate for investigating the effects of IMF sector structure on the cusp, but not for assessing the influence of magnetopause reconnection. Reconnection depends strongly on the sign of B_Z, and the magnetosphere responds to changes in the sign of B_Z within minutes [*Slavin*, 2004]. Because the mean value of B_Z is generally smaller than its variability over the averaging intervals, the average IMF is not a good indicator of reconnection dynamics during our cusp transits. We also compared the average IMF before and after each magnetosphere transit to assess IMF stability. Only 18% of orbits that pass through the cusp exhibit an average IMF B_Z that is of the same sign before and after MESSENGER's magnetosphere transit and that is at least one standard deviation different from zero. In contrast, the corresponding percentages for B_X and B_Y are 79% and 42%, respectively. The data set therefore allows reliable assessment of the cusp dependence on IMF B_X, which at Mercury's orbit is the dominant IMF component and is predicted to have a strong influence on pressures in the cusp [e.g., *Sarantos et al.*, 2001]. Determining the variability in cusp location and pressure due to dynamics associated with magnetopause reconnection, as indicated by the IMF B_Y and B_Z components, is left for future analyses.

[14] We assessed the influence of the IMF B_X and the solar wind ram pressure on the cusp plasma pressure as follows. Statistics were evaluated separately for ascending and descending passes and for positive and negative IMF B_X, because an anti-sunward IMF (negative B_X) is expected to facilitate plasma transport into the northern cusp [e.g., *Sarantos et al.*, 2001]. The ascending tracks were divided approximately equally between positive and negative B_X, but the magnitude of B_X was ~1.7 times higher for sunward than for anti-sunward IMF conditions. The results indicate a larger plasma pressure in the cusp for negative B_X. The high-altitude datasets for $B_X > 0$ and $B_X < 0$ have similar mean altitudes and mean ram pressure (P_{Ram}) values, so the 40% deeper magnetic pressure deficit for negative than positive B_X can be attributed to the IMF orientation. Variation in the cusp mean position at Mercury for the different signs of B_X and comparable average P_{Ram}, as on the ascending tracks, is at most ~0.5° compared to the average cusp extent of ~11°.

[15] We performed SEA on $P_{B\text{-deficit}}$ for each of the two ascending-track populations following the procedure described in Section 2, except that outside the depression interval we padded the $P_{B\text{-deficit}}$ values with zeroes to fill out the time to 8 min for each event (Figure 1, bottom). The SEA profiles of $P_{B\text{-deficit}}$ (Figure 4) confirm that the magnetic pressure deficit in the cusp for the transits with $B_X < 0$ is, on average, larger in magnitude than for $B_X > 0$ and show that the cusp is present regardless of the sign of B_X. The sunward/anti-sunward direction of the IMF thus modulates plasma pressures but is not the dominant factor determining pressure in the cusp.

[16] The plasma pressure in the cusp appears to increase with increasing solar wind ram pressure. For $B_X > 0$ the descending tracks exhibit a higher P_{Ram} and also a lower $P_{B\text{-deficit}}$ than the ascending tracks, indicating that the cusp pressures increase with increasing P_{Ram}. The influence of P_{Ram} may account for the smaller difference in $P_{B\text{-deficit}}$ between the descending track observations for $B_X > 0$ and $B_X < 0$, as the mean P_{Ram} is substantially higher for the $B_X > 0$ events. Presumably, $P_{B\text{-deficit}}$ for the $B_X > 0$ descending track cases would have been smaller in magnitude had P_{Ram} for these tracks been comparable to that for the $B_X < 0$ descending track observations.

[17] The estimate of cusp plasma pressures allows us to calculate the average particle flux bombarding the surface. We assume an isotropic particle distribution entering from the well-mixed magnetosheath plasma. By Liouville's theorem, the downgoing phase-space density of particles is preserved along the field line. The surface is a potential sink for particles that will affect the ratio between $P_{B\text{-deficit}}$ and

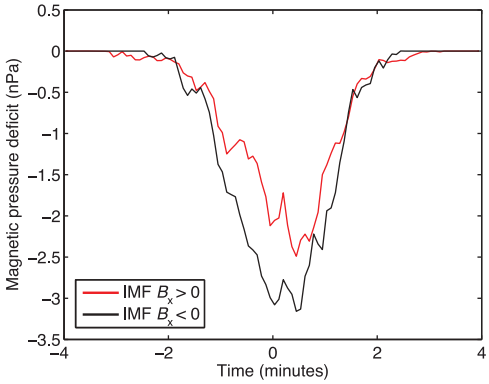

Figure 4. SEA of the magnetic pressure deficit for ascending tracks grouped by IMF $B_X > 0$ (red) and IMF $B_X < 0$ (black). A larger-amplitude magnetic pressure deficit is observed for orbits when the IMF has a negative, or anti-sunward, B_X component.

the downgoing particle flux by depleting the upgoing population. We consider two limits: particles are either perfectly reflected or completely lost at the surface. The average magnetic field strengths on the ascending (B_0 = 186 nT) and descending (B_1 = 312 nT) passes and the estimate of the surface field (B_s = 503 nT) allow us to estimate the ratio between the downgoing pressure and $P_{\text{B-deficit}}$ under the assumption that pitch angles that mirror below the surface are lost from the upgoing portion of the phase-space density. Since the measured magnetic pressure deficit is due to the pressure from particle motions perpendicular to the local field direction, we can calculate the ratio between the pressure due to downgoing particles at the surface, P_s, and the perpendicular pressure at the altitude of the ascending tracks, $P_{\perp 0}$. For perfect reflection we find $P_s/P_{\perp 0} = 0.75$, whereas for perfect absorption $P_s/P_{\perp 0} = 0.77$, so that our estimate of the downgoing pressure is insensitive to the surface interaction. From the mean magnetic pressure deficit along the high-altitude ascending tracks, we find $P_{\perp 0}$ = 1.79 nPa, and we obtain a P_s of 1.34 to 1.38 nPa, so we take $P_s = 1.36 \pm 0.23$ nPa, where the uncertainty corresponds to 0.76 times half the difference in mean pressures for positive and negative IMF B_X.

[18] For an isotropic gas, the flux of particles through a surface is given by $\Phi = P/\sqrt{(2\pi mkT)}$, where m is the particle mass, T is the temperature, and k is Boltzmann's constant. To estimate the flux of particles to the surface, the surface pressure, P_s, is doubled to account for the upgoing half of the distribution. We assume that the plasma is dominated by protons, so $m = m_p$, and we use a characteristic energy of particles in the cusp of 1.05 $\pm$ 0.95 keV from FIPS data (since FIPS observed particles with energies between 0.1 to 2 keV in the cusp) [*Zurbuchen et al.*, 2011]. These assumptions yield an average surface flux of $\Phi_s = (2.1 \pm 1.0) \times 10^{12}$ particles m^{-2} s^{-1}. This value agrees with the average flux over perihelion and aphelion conditions of $\sim 3 \times 10^{12}$ particles m^{-2} s^{-1} predicted by *Sarantos et al.* [2007]. We estimate the total number of particles that hit the surface in the cusp region by projecting the area of the cusp at the altitude of the descending tracks down to the surface. We calculate an upper and a lower limit for the area. Our lower limit is estimated from the area A of a trapezoid that encompasses the minimum region over which the cusp is observed at the altitude of the descending tracks in Figure 3, projected down to the surface, using $A \propto 1/B$. Our upper limit is estimated by taking a circular area of radius equal to half the maximum latitudinal extent of the cusp at the lower altitudes, and again projecting this down to the surface. The mean cusp area at the surface is then $(5.2 \pm 1.6) \times 10^{11}$ m^2, centered at 74.7° MSO latitude on the surface, and we find that $(1.1 \pm 0.6) \times 10^{24}$ particles bombard the northern cusp region every second. The uncertainty in our total flux is primarily from the uncertainties in the proton temperature and the area of the cusp.

[19] As a check on the validity of Liouville's theorem we compared the pressures estimated for the ascending and descending tracks. For complete surface absorption, the ratio of the perpendicular pressures at the two altitudes should be $P_{\perp 1}/P_{\perp 0} = 0.93$, so we expect the pressure ratio to be between 0.93 and 1. For IMF $B_X < 0$, under which solar wind P_{Ram} values are comparable between ascending and descending tracks (Table 1), the pressures are the same to within the uncertainties.

[20] Because of the northward offset of Mercury's dipole, and the resulting weaker surface magnetic field at high southern than northern latitudes, we expect the flux of precipitating particles to occur over a larger area in the southern cusp region than in the north. In the absence of observations of the southern cusp, we use the offset of the dipole magnetic field to estimate the total number of particles reaching the surface in the south. We calculate the central MSO latitude of the southern cusp to be about 64°S. The magnetospheric model [*Anderson et al.*, 2011] predicts a surface field strength at this latitude of 158 nT. From the ratio of the model surface field strength in the south to that in the north we estimate that the cusp area in the south is 2×10^{12} m^2, and the number of particles reaching the surface in the southern cusp region is correspondingly higher, 4×10^{24} particles s^{-1}. Over a Mercury solar day, the planetary surface rotates under the cusp, so the cusp precipitation reaches all planetary longitudes in a band extending $\sim$1600 km ($\sim$38°) in latitude. The IMF B_X effect we observe here, corresponding to 40% higher pressures in the northern cusp for negative than for positive IMF B_X, implies that the flux to the southern cusp should dominate regardless of the IMF direction. These hemispheric flux differences would lead to a persistently greater exospheric source from the south, as sputtering is most likely a contributing factor in populating the exosphere of Mercury [*Sarantos et al.*, 2007]. In addition, if solar wind ion sputtering is a dominant source of space weathering at Mercury, this signature may be observed in surface reflectance spectra. It is, however, possible that Mercury's current magnetic field configuration has not been in place sufficiently long compared with space weathering timescales for this hemispheric asymmetry to be evident in surface reflectance and color differences. Alternatively, the surface may already have reached saturation, in which case hemispheric differences will be muted.

4. Conclusions

[21] From six months of MESSENGER MAG observations we have characterized Mercury's northern cusp region and found that it is persistently present but variable in extent and in the depth of its magnetic field depression. We focused on the role of the IMF B_X direction and the solar wind ram pressure in modulating the average plasma pressure in the cusp because of possible observable consequences for exospheric processes and space weathering. The northern cusp is clearly evident even during sunward IMF conditions but exhibits 40% higher plasma pressures on average during anti-sunward conditions, indicating that the effect of IMF B_X direction is present. Rapid variability in cusp pressures and orbit-to-orbit variations in the latitudinal extent of the cusp may be related to magnetospheric dynamics associated with southward IMF conditions. We estimate that on average $(1.1 \pm 0.6) \times 10^{24}$ protons per second reach Mercury's surface in the northern hemisphere cusp region, thus (via sputtering) contributing a source for the exosphere. Because of the northward offset of the planetary dipole, the flux of particles bombarding the southern cusp should be a factor of 4 higher, yielding a greater exospheric source in the south. Similarly, space weathering in the south due to cusp precipitation should occur over an area 4 times larger than in the north (or equivalently, over a latitudinal extent that is a factor of two larger). The implications of the north-south

magnetic asymmetry for exospheric dynamics are therefore substantial and warrant efforts to confirm the estimated difference in surface magnetic field intensities. Whether a north-south asymmetry is evident in surface reflectance differences depends on the length of time that the present north-south asymmetry in the magnetic field has been maintained.

[22] **Acknowledgments.** The MESSENGER project is supported by the NASA Discovery Program under contracts NAS5-97271 to The Johns Hopkins University Applied Physics Laboratory and NASW-00002 to the Carnegie Institution of Washington. CLJ and MEP are supported by MESSENGER Participating Scientist grants NNX11AB84G and NNH08CC05C. RMW and CLJ acknowledge support from the Natural Sciences and Engineering Research Council of Canada. We thank two anonymous reviewers for helpful comments on an earlier version of this paper. We also thank the Community Coordinated Modeling Center for providing ENLIL model runs.

[23] The Editor thanks Anna Milillo and an anonymous reviewer for assisting with the evaluation of this paper.

References

Alexeev, I. I., et al. (2010), Mercury's magnetospheric magnetic field after the first two MESSENGER flybys, *Icarus*, *209*, 23–39, doi:10.1016/j.icarus.2010.01.024.

Anderson, B. J., M. H. Acuña, D. A. Lohr, J. Scheifele, A. Raval, H. Korth, and J. A. Slavin (2007), The Magnetometer instrument on MESSENGER, *Space Sci. Rev.*, *131*, 417–450, doi:10.1007/s11214-007-9246-7.

Anderson, B. J., C. L. Johnson, H. Korth, M. E. Purucker, R. M. Winslow, J. A. Slavin, S. C. Solomon, R. L. McNutt Jr., J. M. Raines, and T. H. Zurbuchen (2011), The global magnetic field of Mercury from MESSENGER orbital observations, *Science*, *333*, 1859–1862, doi:10.1126/science.1211001.

Delcourt, D. C., S. Grimald, F. Leblanc, J.-J. Berthelier, A. Millilo, A. Mura, S. Orsini, and T. E. Moore (2003), A quantitative model of planetary Na^+ contribution to Mercury's magnetosphere, *Ann. Geophys.*, *21*, 1723–1736, doi:10.5194/angeo-21-1723-2003.

Ip, W.-H., and A. Kopp (2002), MHD simulations of the solar wind interaction with Mercury, *J. Geophys. Res.*, *107*(A11), 1348, doi:10.1029/2001JA009171.

Kabin, K., T. I. Gombosi, D. L. DeZeeuw, and K. G. Powell (2000), Interaction of Mercury with the solar wind, *Icarus*, *143*, 397–406, doi:10.1006/icar.1999.6252.

Kallio, E., and P. Janhunen (2003), Solar wind and magnetospheric ion impact on Mercury's surface, *Geophys. Res. Lett.*, *30*(17), 1877, doi:10.1029/2003GL017842.

Korth, H., et al. (2011a), The interplanetary magnetic field at Mercury's orbit, *Planet. Space Sci.*, *59*, 2075–2085, doi:10.1016/j.pss.2010.10.014.

Korth, H., B. J. Anderson, J. M. Raines, J. A. Slavin, T. H. Zurbuchen, C. L. Johnson, M. E. Purucker, R. M. Winslow, S. C. Solomon, and R. L. McNutt Jr. (2011b), Plasma pressure in Mercury's equatorial magnetosphere derived from MESSENGER Magnetometer observations, *Geophys. Res. Lett.*, *38*, L22201, doi:10.1029/2011GL049451.

Lavraud, B., et al. (2005), Cluster observes the high-altitude cusp region, *Surv. Geophys.*, *26*, 135–175, doi:10.1007/s10712-005-1875-3.

Massetti, S., S. Orsini, A. Milillo, A. Mura, E. De Angelis, H. Lammer, and P. Wurz (2003), Mapping of the cusp plasma precipitation on the surface of Mercury, *Icarus*, *166*, 229–237, doi:10.1016/j.icarus.2003.08.005.

Massetti, S., S. Orsini, A. Milillo, and A. Mura (2007), Modelling Mercury's magnetosphere and plasma entry through the dayside magnetopause, *Planet. Space Sci.*, *55*, 1557–1568, doi:10.1016/j.pss.2006.12.008.

Mura, A., S. Orsini, A. Milillo, D. Delcourt, S. Massetti, and E. De Angelis (2005), Dayside H^+ circulation at Mercury and neutral particle emission, *Icarus*, *175*, 305–319, doi:10.1016/j.icarus.2004.12.010.

Newell, P. T., C.-I. Meng, and D. G. Sibeck (1989), Some low-altitude cusp dependencies on the interplanetary magnetic field, *J. Geophys. Res.*, *94*, 8921–8927, doi:10.1029/JA094iA07p08921.

Newell, P. T., and C.-I. Meng (1994), Ionospheric projections of magnetospheric regions under low and high solar wind pressure conditions, *J. Geophys. Res.*, *99*, 273–286, doi:10.1029/93JA02273.

Odstrcil, D. (2003), Modeling 3-D solar wind structure, *Adv. Space Res.*, *32*, 497–506, doi:10.1016/S0273-1177(03)00332-6.

Omidi, N., X. Blanco-Cano, C. T. Russell, and H. Karimabadi (2006), Global hybrid simulations of solar wind interaction with Mercury: Magnetospheric boundaries, *Adv. Space Res.*, *38*, 632–638, doi:10.1016/j.asr.2005.11.019.

Sarantos, M., P. H. Reiff, T. W. Hill, R. M. Killen, and A. L. Urquhart (2001), A B_x-interconnected magnetosphere model for Mercury, *Planet. Space Sci.*, *49*, 1629–1635, doi:10.1016/S0032-0633(01)00100-3.

Sarantos, M., R. M. Killen, and D. Kim (2007), Predicting the long-term solar wind ion-sputtering source at Mercury, *Planet. Space Sci.*, *55*, 1584–1595, doi:10.1016/j.pss.2006.10.011.

Slavin, J. A. (2004), Mercury's magnetosphere, *Adv. Space Res.*, *33*, 1859–1874, doi:10.1016/j.asr.2003.02.019.

Smith, M. F., and M. Lockwood (1996), Earth's magnetospheric cusps, *Rev. Geophys.*, *34*, 233–260, doi:10.1029/96RG00893.

Trávníček, P. M., P. Hellinger, and D. Schriver (2007), Structure of Mercury's magnetosphere for different pressure of the solar wind: Three-dimensional hybrid simulations, *Geophys. Res. Lett.*, *34*, L05104, doi:10.1029/2006GL028518.

Zhou, X.-W., and C. T. Russell (1997), The location of the high-latitude polar cusp and the shape of the surrounding magnetopause, *J. Geophys. Res.*, *102*, 105–110, doi:10.1029/96JA02702.

Zhou, X.-W., C. T. Russell, G. Le, S. A. Fuselier, and J. D. Scudder (2000), Solar wind control of the polar cusp at high altitude, *J. Geophys. Res.*, *105*, 245–251, doi:10.1029/1999JA900412.

Zurbuchen, T. H., et al. (2011), MESSENGER observations of the spatial distribution of planetary ions near Mercury, *Science*, *333*, 1862–1865, doi:10.1126/science.1211302.